# Nanopixel Waveguide Polarization Rotator Towards Integrated CRDS Breath Sensor for Self-Lasing Suspension

Sara Bruhier
Interdisciplinary Graduate School of Engineering Sciences, Kyushu University

Jiang, Haisong
Interdisciplinary Graduate School of Engineering Sciences, Kyushu University

Hamamoto, Kiichi
Interdisciplinary Graduate School of Engineering Sciences, Kyushu University

https://doi.org/10.5109/7323413

出版情報：Proceedings of International Exchange and Innovation Conference on Engineering & Sciences (IEICES). 10, pp.1226-1231, 2024-10-17. International Exchange and Innovation Conference on Engineering & Sciences
バージョン：

# Nanopixel waveguide polarization rotator towards integrated CRDS breath sensor for self-lasing suspension

Sara Bruhier[1], Haisong Jiang[1], Kiichi Hamamoto[1]
Interdisciplinary Graduate School of Engineering Sciences, Kyushu University, Fukuoka, Japan
Corresponding email: bruhier.sara.787@s.kyushu-u.ac.jp

**Abstract:** *In the context of an aging global population, breath analysis offers a non-invasive method to assess health. One approach uses Cavity Ring-Down Spectroscopy (CRDS), where an optical amplifier compensates for feedback loop loss. However, the self-lasing phenomenon (arising when coherency is secured at a wavelength other than the sensing light) reduces device sensitivity. To mitigate this, a polarization rotator is introduced in the ring cavity, ensuring amplification benefits only the sensing light. As we develop an integrable CRDS system on a Silicon-On-Insulator (SOI) platform, we demonstrate that a 90° polarization rotation is crucial. SOI nanopixel waveguides with two converters and air holes can achieve an 86° to 94° rotation over a 20-nm wavelength range, with insertion loss manageable by the EDFA. A hole diameter of 70 nm offers a balance between reduced loss and efficient mode conversion, though larger holes may enhance mode confinement, particularly for TE10 and TM00 modes.*

**Keywords:** breath sensing, polarization rotator, photonics integrated circuit, nanopixel waveguide

## 1. INTRODUCTION

As reported by the World Health Organization decade study, the global population ages more and more rapidly [1]. Self and daily health monitoring has therefore gained interest to maintain people's vitality and ensure "healthy ageing". However, assessing one patient's condition often involves the use of invasive methods, which implies the puncturing of the skin or entering the body such as with blood tests, biopsies, and endoscopies [2]. They often serve as important indicators that guide towards but may not always provide diagnosis on their own and tend to induce stress in patients [3]. In the evolving landscape of predictive and precision medicine, minimizing patient discomfort and enhancing the efficiency of diagnostic procedures are increasingly vital considerations [4]. Because disease markers can be found in breath, one solution relies on human exhaled breath analysis. The concentration of these components increases when a person suffers from a disease in a specific location even at an early stage, and advances in early detection and treatment are necessary for certain prevalent diseases such as with lung cancer [5-6].

A chip-sized infrared sensor is investigated to detect breath content. Absorption spectroscopy relies on light as each breath component absorbs a certain wavelength band [7]. Photonic-integrated-circuit-based infrared sensors have been investigated so far to detect breath compounds using absorption spectroscopy [7-9], however, breath sensing requires a very long optical path length for component detection, ranging from several hundred meters to kilometers [8]. A Cavity-Ring-Down Spectroscopy (CRDS) system ensures ppm-order gas detection [10], and we have realized CRDS by using loop-configuration instead of mirroring configuration. Due to the long optical path length, an optical amplifier is required to compensate the loss to ensure long effective sensing path (the sensing light can propagate more roundtrips in the ring cavity). Nevertheless, the loop structure results in unwanted peaks in wavelengths at different locations than the sensing wavelength one because of a self-lasing phenomenon whose mechanics will be explained in this study. Previous work shows experimentally that inserting a polarization rotator inside the loop is one effective method to obtaining higher sensitivity of the device [10-12].

Our research goal is to provide a prototype for compact breath sensing with a Photonics Integrated Circuit integration (PIC). Controlling polarization light state in the PIC is thus crucial to prevent sensitivity loss due to self-lasing in the CRDS loop. In this study, we will explain the CRDS system principle and how the optical amplifier inside the loop leads to self-lasing. We will present and discuss the currently available methods to tackle this issue by suspending the light coherency inside the ring cavity. We will show our design approach of a polarization rotator with nanopixel waveguide structure as this approach is suitable for the means of integrability and minimum loss introduction. Finally, we will show that a 90° rotation is necessary for self-lasing suspension in the CRDS system and that SOI nanopixel waveguide using 2 converters with air holes can achieve the corresponding birefringent medium to operate an 86 to 94° rotation on a 20-nm wavelength range with an insertion loss lower than 5 dB, sufficient for the EDFA to compensate. Hole diameter of 70 nm offers a balance between reduced loss and efficient mode conversion, though larger holes may enhance mode confinement, particularly for TE10 and TM00 modes.

## 2. CRDS SYSTEM

### 2.1 Principle

Cavity Ring-Down Spectroscopy or CRDS relies on the direct absorption properties of gas molecules defined by both their spectrum (main absorption wavelength peak) and their cross-section. Direct absorption is a linear spectroscopic technique making it straightforward to quantify as it scales proportionally with both molecular number density and absorption strength. This linearity ensures that it performs well across a wide range of molecular absorption concentrations and absorption cross-sections [[14].

We are working on an amplified-CRDS scheme presented in Fig. 1 [[13]. A laser diode (LD) injects a

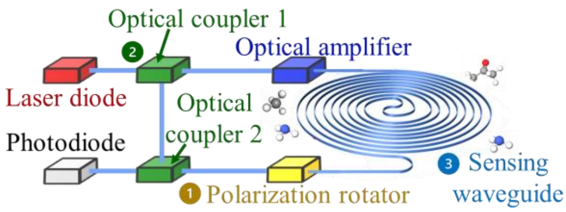


Fig. 1. Cavity Ring-Down Spectroscopy breath sensing system schematics [11].

pulses train, referred as the sensing light, at a wavelength λ that corresponds to the main absorption wavelength peak of the gas molecule to detect. Two optical couplers take the role of high-reflective mirrors that delimits the ring cavity. Coupler 1 is 50:50 to balance between the injection light intensity from the LD and the guided back light intensity from coupler 2. Coupler 2 guides back most of the sensing light (90%) to the feedback loop. Long sensing path is secured by the sensing waveguide inserted inside the ring cavity. The evanescent field of the sensing waveguide enables the gas-light interaction [[12]. The photodiode collects the CRDS pulses, and their number is correlated to the gas concentration inside the cavity as detailed in [13]. To detect higher number of pulses enabling higher CRDS sensitivity, an optical amplifier (Erbium Doped Fiber Amplifier, EDFA) compensates the total loss of the CRDS system (propagation, coupling and insertion losses mainly) to allow the sensing light to travel more roundtrips in the cavity, thus, to detect more pulses. We will explain in the following section why the polarization rotator plays a crucial role in suspending what we refer to as self-lasing phenomenon.

### 2.2 Self-lasing issue

The total experimental system loss is measured at 24.7 dB. Thus, the EDFA will compensate this loss with a minimum gain of 24.7 dB, achieved for a minimum pumping current of 340 mA. Sensing light is here considered at λ = 1572 nm (in case of the carbon dioxide detection). A self-lasing phenomenon has been experimentally observed (Fig.2.), however, for an injected current for the pumping laser diode in the EDFA above 100 mA at λ = 1564 nm (case of high pumping condition) [15].

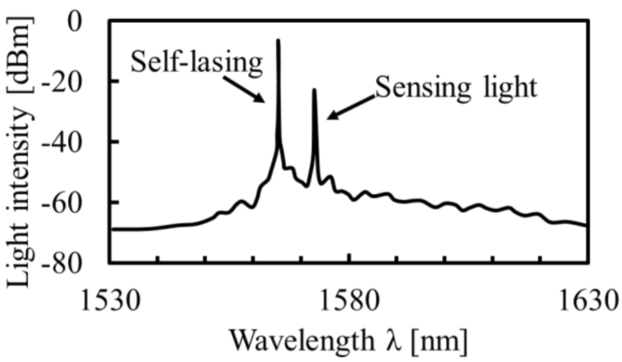


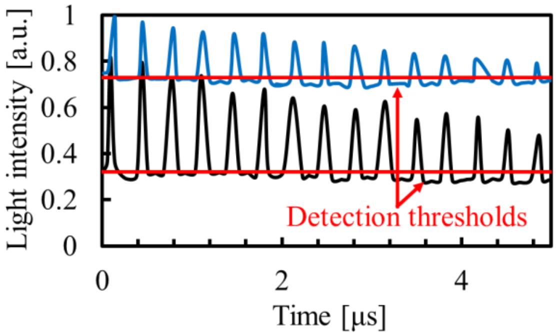


Fig. 2 Self-lasing phenomenon in CRDS system due to EDFA gain for carbon dioxide detection (λ = 1572 nm for the sensing light); (a) Optical spectrum of CRDS system with self-lasing and sensing light peaks (EDFA gain of 10 dB for the black curve, and 20 dB for the blue); (b) Impact on CRDS pulses intensity with increased background noise

Since the pumping current of EDFA must be higher than 340 mA to compensate the CRDS system loss, the self-lasing phenomenon will occur in such conditions. This is explained by the Amplified Spontaneous Emission produced by the population inversion in EDFA that travels inside the CRDS feedback loop, gets the coherency condition secured and thus leads to a lasing at a different wavelength. This coherency condition or "resonance" is a necessary requirement to obtain oscillations in cavity (here we work with ring-cavity), but it is not a sufficient one. For this reason, self-lasing phenomenon need to be suspended.

## 3. COHERENCY SUSPENSION METHODS

Disrupting the light coherency in passive Silicon-On-Insulator (SOI) waveguide involves various techniques that alter the phase relationships, scatter light, or introduce other disturbances. Not all of them are suitable, especially if they introduce extra optical loss as it is a critical consideration in the CRDS system or if they require external control (active devices) which would not apply for the sensor integration on a photonics chip. Also, the chosen method requires compact footprint. Indeed, if the available area for the sensing waveguide is bigger, the sensing path will be extended and thus the detection sensitivity will be enhanced.
We present in the following section several methods of coherency disruption suited for PICs using passive and static (not mechanically reconfigurable) SOI-based optical sub-system. We will show that polarization rotator is the chosen candidate to remove the self-lasing phenomenon in our breath sensor.

### 3.1 Light scattering introduction

Introducing light scattering would disturb the light coherency, however, at the cost of additional excess loss. There are different ways to induce lights scattering, such as surface roughness on the waveguide, or by introducing random refractive index variation [16-18]. These two methods fall within the scope of "disordered waveguides".
Grating structures ("ordered waveguides") could also lead to light scattering for example with uniform gratings structures such as photonics crystal structures or Bragg gratings (with higher relative scattering loss) [19], or

with defined non-uniform gratings or even randomized periods to multiply the light scattering directions thus reducing the coherence. In any case, the induced phase shift will be inherent to the grating structure (uniform or not), thus will be invariant across time (i.e., cavity roundtrips). These methods could be defined as a phase gain applied to the sensing light injected in the considered structure. However, as we will see in the following paragraph, this constant phase shift will eventually satisfy the coherency condition if working for a higher number of pulses to reach higher detection sensitivity, and the self-lasing phenomenon will occur.

### 3.2 Interferometers

Spatial mode mixing could control destructive interferences thus killing the light coherency, for instance with a Mach-Zehnder type. With asymmetrical interferometer arms (different lengths), a phase shift can be applied which would disrupt the coherency between the two optical paths after their recombination at the Mach-Zehnder interferometer's output.

### 3.3 Absorption introduction

Absorptive elements would introduce amplitude noise, so indirectly influence the phase coherence. However, the system loss is a critical aspect of the device sensitivity. The additional background noise would affect the detection threshold set for the pulses number evaluation (as mentioned in Fig. 2) thus affect the gas concentration evaluation.

### 3.4 Chirp introduction

Introducing a chirp in an SOI waveguide by varying its width can broaden the spectrum of the light propagating through it, thereby reducing its coherence. This technique works by gradually changing the waveguide width, which alters the effective refractive index along the propagation path. As a result, different frequency components of the light experience different phase velocities, leading to a chirp (a frequency-dependent phase shift) that spreads the spectral components.

However, in a ring cavity, each round trip of light through the chirped section will further modulate the phase. The waveguide being a part of the feedback loop, the cumulative effect of multiple round trips could lead to significant spectral broadening, as shown in this study for propagation length greater than 1 cm [20].

We will detail in the following section the chosen method for suspending the self-lasing peak in the CRDS loop, by rotating the polarization light state by a 90° angle. We will show that nanopixel is a suitable waveguide structure for our integrated CRDS sensor application.

## 4. POLARIZATION ROTATOR

### 4.1 Requirements

In order to suspend the light coherency to prevent any self-lasing, the Polarization Rotator (PR) must perform ideally a 90° rotation angle of the sensing light. On one hand if the sensing light mode is orthogonal to the PR output mode, i.e. their signals are in perfect phase opposition, the coherent condition cannot be secured. On the other hand, in case the output from the PR is different from 90°, a non-zero TE component will persist at the PR output. As it is travelling many roundtrips inside the CRDS loop, it will eventually interfere constructively with the sensing light mode, satisfying the coherency condition for the traveling optical wave thus leading to self-lasing.

In addition to this, the insertion loss (propagation and coupling loss) should not be higher than 5 dB, so that the EDFA gain can compensate the total loss in the CRDS system with the polarization rotator included.

### 4.2 Birefringence with nanopixel waveguide

In birefringent waveguides or waveguides with anisotropic materials, polarization modes can couple and exchange energy. So, to reach higher mode conversion efficiency, we should work with guiding medium with birefringence. This is the reason why asymmetric waveguides such as with varying core index, or asymmetric geometry (cornered-etched core) are researched for polarization rotation. There are also magneto-optic effects which states that in the presence of a magnetic field, the polarization states are influenced, causing coupling through the Faraday effect. However, we aim at designing a passive PR.

Hole etching inside a Silicon waveguide core introduces an anisotropic property to the core medium, therefore becoming a birefringent medium.

### 4.3 Induced birefringence by nanopixel structure

The core thickness was studied for h = 220 nm. In a birefringent medium, light propagates with different speeds depending on its polarization state due to different refractive indices for orthogonal polarizations. This leads to a phase difference between the two polarization components as they travel through the medium. The polarization beat length is the distance along the waveguide or fiber at which the accumulated phase difference between the orthogonal polarization modes equals $2\pi$. At this distance, the relative phase shift causes the polarization state to return to its initial orientation. For an accumulated phase θ, a general expression is given by eq.(1):

$$\theta = \frac{\pi L \Delta n}{\lambda} \qquad (1)$$

where Δn represents the difference in effective refractive index between TE and TM modes in the waveguide, and λ the light wavelength. Its derivative as regard to the wavelength is defined by this equation:

$$\frac{d\theta}{d\lambda} = -\frac{\pi L \Delta n}{\lambda^2} \qquad (2)$$

To obtain a 90° rotation, we need to consider polarization half-beat length as defined in this equation (by simply replacing θ with π/2 rad) in case of a waveguide with no etched holes referred later as "empty waveguide:

$$L_{\pi/2} = \frac{\lambda}{2\Delta n} \qquad (3)$$

If using an SOI waveguide, the difference in effective refractive indexes Δn for the TE and TM modes has the potential to be greater due to a strongly guiding waveguide. With the eq.(3), $L_{\pi/2}$ will be reduced, and so a strongly guiding waveguide serves the purpose of a compact polarization rotator. However, the effective refractive index of the waveguide must be changed in a way or another along the PR so that the input TE00 can slowly be converted towards the TM00 that displays another effective refractive index. Instead of varying the waveguide width such as in adiabatic-tapered PR which needs around 100 μm for high mode conversion efficiency, air holes are etched in the waveguide core to vary locally the effective refractive index while reducing the PR converting length down to around 10 µm-order. We will also consider the area ratio between air hole and the Silicon waveguide core (Si) for a waveguide cross-section (x-y plane) with the following formula (with $N_x$ the number of hole in x-direction):

$$\frac{\text{Air}}{\text{Si}}\text{area} = \frac{d}{w}.N_x \quad (4)$$

We study a nanopixel polarization rotator design based on 2 converters: TE00 converted to TM00 through an intermediate light state with TE10 mode, as described in Fig.3 and in our previous study [19]. The arrangement of air holes will tune locally the effective refractive index to perform the two mode conversions.

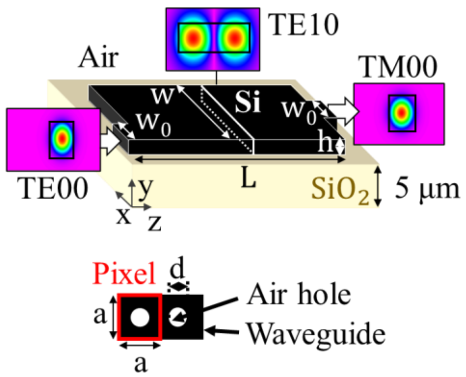


Fig.3. 2-step polarization rotator overall design and air-hole definition

**5. Results & Discussion**

The effective refractive indexes of propagating modes TE00, TE10 and TM00 are calculated using 3D Finite Elements Method (FEM). The polarization rotator thickness is set at h = 220nm. Fig. 3. below represents the evolution of Δn as regard to $L_{\pi/2}$ and the corresponding waveguide width in an empty waveguide.

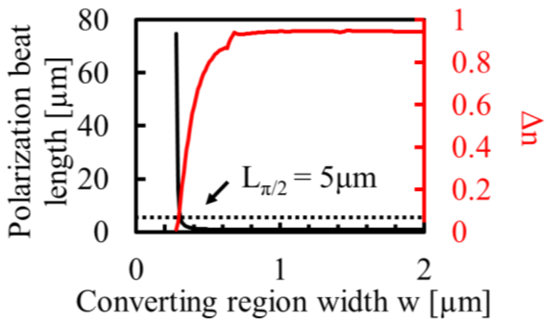


Fig. 3. Difference in effective refractive index between TE and TM modes, and polarization beat length for 90° rotation (eq.(3)) in the empty waveguide as regard to the converter's width (for a core thickness of h = 220 nm)

The graph highlights that increasing the waveguide width enhances the difference in effective refractive indices Δn for different polarization modes (TE00 and TM00), thus reducing the polarization half-beat length and allowing for smaller devices dedicated to PR. However, as the waveguide width approaches approximately w = 0.3 µm, the polarization half-beat length increases dramatically. Selecting a converter width where the Δn between TE00 and TM00 modes stabilizes ensures consistent and reliable polarization conversion performance across the device. However, when Δn is minimized (closer to zero), the phase mismatch between the two modes is reduced, allowing for complete energy transfer from one polarization mode to the other. This ensures that the polarization mode conversion process is both efficient and effective, achieving the desired conversion or rotation. Therefore, to control the birefringence Δn for a given PR converting width (w = 0.96 µm) for smaller $L_{\pi/2}$ (eq.(3)), we study how the air hole arrangement tunes the effective refractive index $n_{eff}$ for different filling defined in Fig. 4 and for the propagating modes in our PR structure: TE00, TE10 and TM00 (Fig. 5.).

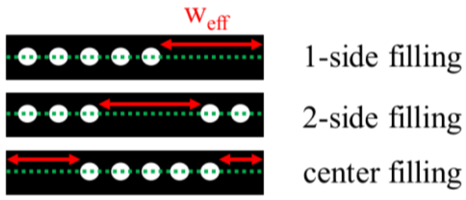


Fig. 4. Arrangement type for 5 air holes filling. Dotted green lines represent the monitored cross-section for FEM simulations (x-y cross-section). Red arrows indicate the available effective waveguide's width $w_{eff}$ for the guided light.

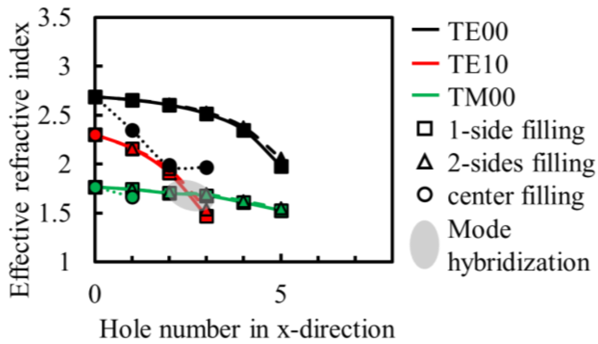


Fig. 5. Impact of 90-nm-diameter hole location in x-direction on local effective refractive index (x-y cross-section, w = 0.96 µm and h = 220 nm)

The holes number and arrangement in the x-direction impact $n_{eff}$ of the propagating modes, however 1-side and 2-sides filling display very similar results. This is explained by the same effective waveguide width $w_{eff}$ available for the light propagation without holes in these 2 configurations (Fig.4.). However, in the case of the center filling, there are two areas with no holes, leaving two possible pathways for guiding the light with reduced $w_{eff}$ for a given number of holes compared with the two other cases. Effective conversion for TE10 to TM00 seems available for a hole number around 2 and 3 (with 90-nm diameter) where Δn ~ 0 and $w_{eff}$ from 630 to 750 nm. This mode hybridization means that the two modes coexist around the same effective refractive index, and this is the case for w ~ 650 nm [19].

In Fig. 6., the local tuning of the refractive index in the x-y plane is also examined by varying the number of etched holes with diameters d ranging from 60 nm (our current fabrication limit for high tolerance on hole diameter) to 120 nm within a pixel size a = 120 nm. We consider here only the case of 2-side fillings. Based on Fig.6., the birefringence for TE00 and TM00 decreases with smaller hole size for an Air/Si area ratio over 20% in the waveguide cross-section. Indeed, smaller holes imply a wider interspace between adjacent holes, thus reducing $w_{eff}$ for available light pathway (in the case of 1 and 2-sides filling arrangement) and probably increases the light scattering in these interspaces. Fig.7. supports this observation in the case of TE10-TM00. Fig.6-8 display the loss for a waveguide length of 5 µm for the propagation of TE00, TE10 and TM00 modes respectively. The length value is chosen based on our current PR device length from [[21]. We note that, in general, the loss increases for a given Air/Si area value with the hole diameter. It appears that d = 70 nm offers a balance for reduced loss while allowing the tuning of Δn closer to zero for the two considered mode conversion.

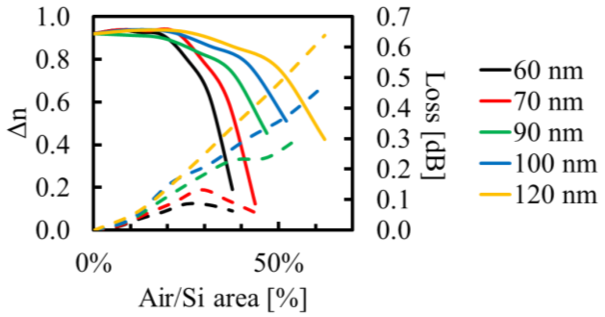


Fig. 6. Difference in effective refractive index between TE00 and TM00 modes (solid lines) and TE00 mode loss (dotted lines, over L = 5 µm) as regard to the air over the silicon area ratio depending on the hole diameter (2-sides filling arrangement, w = 0.96 µm and h = 220 nm)

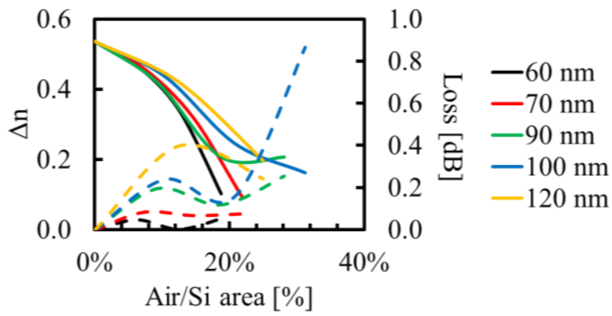


Fig. 7. Difference in effective refractive index between TE10 and TM00 modes (solid lines) and TE10 mode loss (dotted lines, over L = 5 µm) as regard to the air over the silicon area ratio depending on the hole diameter (2-sides filling arrangement, w = 0.96 µm and h = 220 nm)

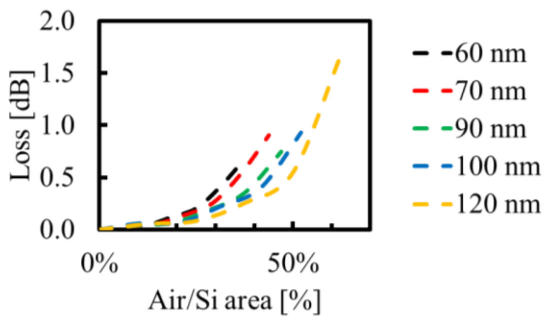


Fig. 8. TM00 mode loss over L = 5 µm as regard to the air over the silicon area ratio depending on the hole diameter (2-sides filling arrangement, w = 0.96 µm and h = 220 nm)

In such configuration w = 0.96 µm and h = 220 nm, we consider that the loss requirement of maximum 5 dB can be satisfied for the different propagating modes involved in the 2-step PR design with air holes for a PR length of 5 µm.

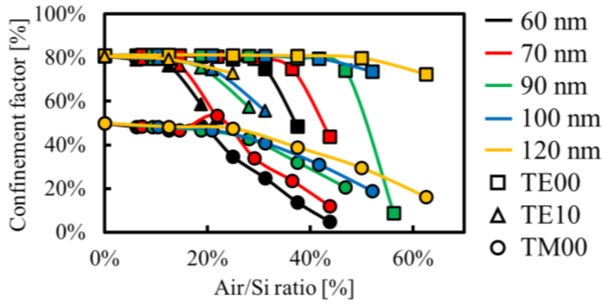


Fig. 9. Confinement factor for the propagating modes TE00, TE10 and TM00 as regard to the air over the silicon area ratio (eq.(2)) depending on the hole diameter (2-sides filling arrangement, w = 0.96 µm, h = 220 nm and a = 120 nm)

In Fig.9., the confinement factor is computed with the 3D-FEM simulations for the propagating modes as regard to the air over the silicon area ratio depending on a given hole diameter. The higher the confinement factor, the better the mode is guided inside the waveguide. Above 15% and 25% of Air/Si ratio respectively, the confinement factor starts to decrease for the TE10 and TM00 modes. Bigger holes diameter enhances the confinement factor for all modes, which needs to be balanced with the birefringence tuning seen previously that performed best with lower loss for d = 70 nm.

As the self-lasing and the sensing wavelength varies experimentally in the CRDS system, it is important that the PR performances cover a certain wavelength range. The variation of the polarization rotation angle over the wavelength is depicted in Fig. 10.

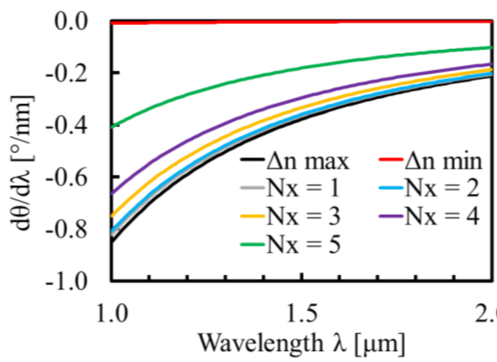


Fig. 10. Variation of polarization rotation angle as regard to wavelength for varying hole number in x-direction $N_x$ (eq.(3)). Δn max and Δn min corresponds to maximum and minimum of Δn for converter's width of 2 µm and 0.27 µm respectively.

With additional air holes, the figure demonstrates that the nanopixel waveguide can support the propagation of TE00 and TM00 modes, enabling 90° polarization rotation. Once the PR design achieves this rotation at λ = 1550 nm, it will maintain effective performance across a wavelength range Δλ = 20nm with a maximum variation for the polarization rotation angle between 86 to 94°.

**6. Conclusion**

In this study, we showed that our CRDS system for breath sensing needs a 90° polarization rotation to suspend a self-lasing phenomenon caused by the use of an optical amplifier (EDFA) inside the ring cavity. We explained that a polarization rotator based on 2 converters with nanopixel waveguide structure can achieve this with air holes tuning birefringence in the SOI core enabling the mode rotation. It can operate an 86 to 94° rotation on a 20-nm wavelength range. Hole diameter of 70 nm potentially offers a balance for reduced loss while allowing the tuning of Δn closer to zero for the TE00-TE10 and the TE10-TM00 mode conversions. However, a balance must be found between higher mode confinement (TE10 and TM00 in particular) allowed by larger holes with the birefringence tuning.

**Acknowledgments**
This work was financially supported by the SECOM Science and Technology Foundation.

**References**
[1] Department of Maternal, Newborn, Child & Adolescent Health & Ageing 2021 Summary Decade of Healthy Ageing: Baseline report ed Institutional Repository for Information Sharing (Geneva: World Health Organization) p. 2, Chap. 1–2
[2] National Cancer Institute 2023, Dictionary of Cancer Terms
[3] Cousins S, Blencowe NS, Blazeby JM., *British Medical Journal Open* **9**-7, e028576 (2019)
[4] S. Licciulli 2023, Cancer Research Catalyst
[5]World Health Organization 2023, June 26 https://who.int/news-room/fact-sheets/detail/lung-cancer?gclid=CjwKCAiAzc2tBhA6EiwArv-i6XxRT1BD-EiHHe8zbKaydMWHX2pGGdJHj2XXJVT_s_aw8uXRb6LxfxoCZsQQAvD_BwE
[6] Jiang B., Xie D., Wang S., Li X. and Wu G., *Frontiers of Genetics* **14**, 1091223 (2023)
[7] N. Gayraud, L.W. Kornaszewski, J.M. Stone, J.C. Knight, D.T. Reid, D.P. Hand, and W.N. MacPherson, "Title," App. Opt., 47(9), 1269-1277 (2008)
[8] D. Nakashima, et.al, "Proposal of Novel Strip High-Mesa Waveguide for Infrared Absorption Sensing" *Applied Physics Express* **5**, 062202 (2012)
[9] Hokazono H., Li W., Enami S., Jiang H. and Hamamoto K., "Gas Sensing Demonstration by Using Silica High-Mesa Waveguide with Amplified Cavity Ring Down Spectroscopy Technique," *IEICE Electronics Express*, **12-10**,.1587/elex.12.20150574 (2015)
[10] Li W., Han Y., Chen Z., Wang L., Jiang H. and Hamamoto K., *Engineering Sciences Reports*, **42**-1, pp. 19–26 (2020)
[11] Li W., Han Y., Chen Z., Wang L., Jiang H. and Hamamoto K., Proceedings of International Exchange and Innovation Conference on Engineering & Sciences (IEICES) **5**, pp.107-108, 2019-10-24
[12] Han Y., W. Li, Jiang H. and Hamamoto K., Proceedings of International Exchange and Innovation Conference on Engineering & Sciences (IEICES). **5**, pp.100-102, 2019-10-24
[13] Li W., Han Y., Chen Z., Wang L., Jiang H., and Hamamoto K., "Amplifier-assisted CRDS (cavity ring-down spectroscopy) toward compact breath sensing," *Japanese Journal of Applied Physics*, **58**-SJ, [SJJD01]. (2019)
[14] Meijer. G, Boogaarts G.H. M., Jongma T.R., Parker. H.D., Coherent cavity ring down spectroscopy, Chemical Physics Letters, **217**-1.2 (1994)
[15] J. Chow, G. Town, B. Eggleton, M. Ibsen, K. Sugden, and I. Bennion, "Multiwavelength generation in an erbium- doped fiber laser using in fiber comb filters", IEEE Photonics Tech. Lett., 8(1), 60-62 (1996).
[16] Shang B., Sun D., Yu P., Wang B., Yu T., Li T., Jiang H., Investigation for Sidewall Roughness Caused Optical Scattering Loss of Silicon-on-Insulator Waveguides with Confocal Laser Scanning Microscopy, Coatings, 10-236 (2020)
[17] Jaberansary. E., Masaud T.M.B., Milosevic M.M., Nedeljkovic M., Mashanovich G.Z., Chong H.M.H., Scattering Loss Estimation Using 2-D Fourier Analysis and Modeling of Sidewall Roughness on Optical Waveguides, IEEE Photonics, **5**-3 (2013)
[18] Gao F., Wang Y., Jia X., Zhang F., Reduction of sidewall roughness in silicon-on-insulator rib waveguides, Applied Surface Science, **252**-14, pp. 5071-5075 (2006)
[19] Li H. An Z., Mao Q., Zuo S., Zhang S., Zhang C., Li E., Garcia J.D.P., SOI Waveguide Bragg Grating Photonic Sensor for Human Body Temperature Measurement Based on Photonic Integrated Interrogator, Nanomaterials (Basel), **12**-1, 29 (2022)
[20] Pakarzadeh H., Akbari F., Propagation of Terahertz Pulses in Photonic Crystal-Based Rib Silicon Waveguides, Silicon, **14**, pp. 2931-2940 (2022)
[21] S. Bruhier, H. Jiang, K. Hamamoto., JJAP, **63**, 07SP01 (2024)